OPTIMAL ORBITS FOR SPARSE CONSTELLATIONS OF MARS NAVIGATION SATELLITES

Todd A. Ely*

Current ideas for Mars navigation constellations range any where from placing telecom/navigation payloads on orbiters that have a primary mission to gather scientific data, to satellite(s) that are dedicated to a telecom/navigation mission. A common denominator to all the ideas being advanced is that the constellations are small in number and provide only discontinuous coverage to Mars surface assets. This contrasts sharply with navigation systems at Earth, such as GPS, that provide continuous, multiple satellite coverage at all Earth surface locations. This study examines orbit selection for small constellations (4 or fewer satellites) at Mars that minimize time to achieve surface position accuracies at specified levels. A genetic algorithm coupled with a computationally efficient navigation metric tool is utilized to conduct the search through the constellation orbit space. The preliminary results indicate that retrograde, mid-altitude (2000 ~ 5000 km) orbits are most efficient. The presented results also quantify the impact that considering orbit error, the largest error contributor can have on surface asset positioning on a global scale.

INTRODUCTION

Recent scientific discoveries at Mars have heralded an unprecedented commitment and focus by NASA and its international partners towards further exploration of Mars. As part of this effort NASA has an on-going project, called the Mars Network, to examine communication and navigation infrastructure requirements needed to support Mars exploration. This potentially could consist of a small constellation of satellites to provide in-situ communication relay and navigation services for other missions at Mars. Current, constellation ideas range any where from placing telecom/navigation payloads on orbiters that have a primary mission to gather scientific data, to satellite(s) that are dedicated to a telecom/navigation mission. A common denominator to all the ideas being advanced is the constellations are small in number and provide only discontinuous coverage to Mars surface assets. This contrasts sharply with navigation systems at Earth, such as GPS, that provide continuous, multiple satellite coverage at all Earth surface locations. A natural question that arises when considering surface asset positioning is "What is the

* Senior Engineer, Navigation and Mission Design Section, Jet Propulsion Laboratory, California Institute of Technology, Pasadena, CA 91109.

best orbit for position determination using Doppler or range tracking measurements?" Even though the question is simply stated, the problem it poses is actually quite complex to answer, especially when coverage is discontinuous. This is true even when considering a simplified problem that focuses only on geometry related issues, i.e., realistic error sources such as orbit knowledge, atmosphere delays, are neglected. Fundamentally, the problem involves the relative geometry between surface stations and the in-view satellites at specific times, the tangent space of the geometry (i.e., partials of slant range with respect to nominal states), and the selected initial conditions. Indeed, it is sufficiently complex that no generalized, analytical results are known to the author. In order to analyze global positioning services to surface assets numerical simulations must be employed.

Typically high fidelity navigation analysis tools are capable of examining only a single scenario at a time. That is, given a surface location, satellite orbit(s), and initial times, the tool can give detailed information regarding positioning performance for the given location and times. Unfortunately, this information is not readily generalized to other locations, orbits, and times. Tools specifically geared towards assessing the global positioning performance need to use simplified models so that statistical data regarding positioning accuracy to a distributed set of ground locations can be collected in a *meaningful* amount of time. Ely, et. al., [1] conducted analysis of this type to arrive at candidate constellations for the Mars Network. However, orbit selection proceeded in an ad hoc manner, and was very manpower intensive. In the current study, a systematic optimization methodology using a genetic algorithm (GA) is utilized to find sparse constellations that globally minimize selected metrics that are related to the performance of a constellation at providing surface asset position determination services. An example metric is the average time it takes to collect sufficient tracking data between a surface asset and the constellation in order to determine the surface asset's position to within some prescribed accuracy. This function is called the Mean of the Position Accuracy Response Time (MPART). An example optimization objective is to minimize sum of the spatial average of MPART over all stations that are distributed across the planet and the standard deviation associated with this average. Doing so not only minimizes average MPART values for all stations, but minimizes their variations across latitude and longitude.

MARS NETWORK MEASUREMENT DATA

The proximity link navigation system being proposed for use at Mars will nominally employ Doppler and slant range measurements to perform surface asset positioning services. In particular, 2-Way Doppler collected by Mars Network satellites is the default data type because it minimizes the complexity of the surface asset's tracking hardware (i.e., only a coherent transponding capability is needed) without sacrificing data accuracy. The Mars Network payload will also be able to formulate range measurements, but ensuring an accurate data type imposes requirements on the surface assets to have a

more sophisticated transceiver. The Network payload will also carry an ultra stable oscillator (USO) that has a short term Allan deviation that is better than $1x10^{-12}$. This oscillator enables the Network to provide precise timing services and, for users that are equipped with a similar USO, very precise 1-Way Doppler and range measurement types. However, since the default surface asset will rely on 2-Way Doppler as the primary in-situ measurement type, it is this type that is used in the subsequent constellation design studies.

Fundamentally, assessment of positioning performance is ascertained by analyzing the geometry of the slant range between surface assets and the satellites that comprise the orbiting constellation. The instantaneous slant range vector is defined as,

$$\vec{\rho}(t) = \vec{r}^{\,sc}(t) - \vec{r}^{\,sa}(t) \tag{1}$$

where $\vec{r}^{\,sc}$ is the position vector of a spacecraft at time t, and $\vec{r}^{\,sa}$ is the position vector of a surface asset at the same time. The magnitude of this vector, identified by ρ , is the scalar-valued slant range between the two. Moyer [2] defines 2-Way Doppler that is collected by the originating transceiver element (i.e., the Mars Network payload) over a count time interval $T_c = t_e - t_s$ (e refers to end and s to start) as,

$$\Delta F_2 = \frac{M f_T(t_1)}{\Delta t} \int_{T_c} \left(1 - \frac{f_R(t)}{f_T(t)} \right) dt \ , \tag{2}$$

where M is the frequency turnaround ratio of the tranponding element (i.e. the surface asset), $f_T(\cdot)$ is the transmission frequency, $f_R(\cdot)$ is the received frequency (which includes the instantaneous 2-Way Doppler shift), t_1 is the time of transmission, and the integration is over the count time interval T_c and begins after reception of the signal originally transmitted at t_1. This exact formulation can be approximated with sufficient accuracy for in-situ navigation purposes using instantaneous ranges as follows,

$$\Delta F_2(t_e) = \frac{2Mf_T}{cT_c} \left\{ \rho(t_e) \left[1 + O\left(\left| \frac{v^{sc,\,sa}}{c} \right| \right) \right] - \rho(t_s) \left[1 + O\left(\left| \frac{v^{sc,\,sa}}{c} \right| \right) \right] \right\} \approx \frac{2Mf_T}{cT_c} \left[\rho(t_e) - \rho(t_s) \right] \ ,$$

(3)

where the transmission frequency has been assumed constant, and relativistic delays and media transmission delays have been neglected. Finally, assuming the count time T_c is short, the Doppler measurement can be related to an instantaneous range rate using,

$$\Delta F_2(t_e) = \frac{2Mf_T}{c}\left[\dot{\rho}(t_e) + O(\ddot{\rho}\Delta t)\right] \approx \frac{2Mf_T}{c}\dot{\rho}(t_e) = \frac{2Mf_T}{c}\frac{\bar{\rho}\cdot\dot{\bar{\rho}}}{\rho}\Bigg|_{t_e} . \quad (4)$$

The range difference formulation for Doppler has been selected for implementation because it yields greater accuracies (versus range rate) when the slant ranges become large (i.e., using the Mars Network proximity payload for navigation support of Mars approaching spacecraft) or when count times become large. For convenience this study utilizes the range difference portions of Eqs (3) for analysis, hence the observation of interest takes the form,

$$DR(t_e) \equiv \left[\rho(t_e) - \rho(t_s)\right] \approx \dot{\rho}(t_e)T_c . \quad (5)$$

Note that the range rate approximation shown in Eq. (5) is used later for an orbit error consider analysis. The equivalent noise statistic for $DR(\cdot)$ defined in Eq. (5) takes the form,

$$E[DR(t_i)] = 0, \qquad E\left[DR(t_i)DR(t_j)\right] = (\sigma_{DR})^2\delta_{ij} \rightarrow \sigma_{DR} = \sigma_{\dot{\rho}}T_c = \sigma_{\Delta F_2}\frac{cT_c}{2Mf_T} . \quad (6)$$

For this study, $\sigma_{DR} = 17$ mm $(\rightarrow \sigma_{\dot{\rho}} = .28$ mm/s & $T_c = 60$ sec , $\sigma_{\Delta F_2} = .8$ mHz @ UHF) has been selected for use.

A NAVIGATION METRIC FOR SPARSE CONSTELLATION DESIGN

Sparse constellations are characterized by the visibility between a surface asset and the satellite constellation as not being continuous, and typically involve only a single, in-view satellite at a time. It is possible to encounter multiple satellites in-view at the same time, but this is an atypical event. This realization motivates the choice for a metric that measures the performance of surface asset positioning services provided by competing constellation designs to account not only for accuracy, but the elapsed observation time needed to achieve the computed accuracy, as well. Furthermore, since the relative slant range geometry of a surface asset and the constellation is changing, the metric based on this geometry requires statistical sampling over a sufficient collection period such that it can achieve a stationary value. The metric selected is the average time it takes to collect sufficient tracking data between a surface asset and the constellation in order to determine the surface asset's position to within some prescribed accuracy. This function is called the Mean of the Position Accuracy Response Time (MPART), and can be expressed as a function of surface asset longitude λ and latitude L as follows,

$$MPART(\lambda,L) = \frac{1}{N}\sum_{i=1}^{N}\Delta t_i(\lambda,L) \quad , \tag{7}$$

such that,

$$\Delta t_i(\lambda,L) \mapsto \sqrt{P_{xx}(\lambda,L,\Delta t_i)+P_{yy}(\lambda,L,\Delta t_i)+P_{zz}(\lambda,L,\Delta t_i)} < RSS_{\text{desired}} \ . \tag{8}$$

The epoch time for sample i where measurement collection begins for this sample is identified as $t_{o,i}$, and $\Delta t_i = (t_i - t_{o,i})$ is the sample time interval needed to obtain sufficient tracking to a surface asset located at (λ, L) to determine its epoch state covariance components $\{P_{xx}(\Delta t_i), P_{yy}(\Delta t_i), P_{zz}(\Delta t_i)\}$ such that their RSS value is less than a specified threshold $RSS_{desired}$. For the results that follow the value for $RSS_{desired}$ has been set at 1 m, unless otherwise noted. Note, that for each sample Δt_i the apriori covariance associated with the surface asset is specified at some level and is denoted by $\mathbf{P}_o$, where for this study, $diag(\mathbf{P}_o) = (P_{xx,o}, P_{yy,o}, P_{zz,o})$ = (10 km, 10 km, 10 km) and the off diagonals are zero.

Computation of the MPART metric proceeds by propagating the constellation, composed of N_{sc} spacecraft, forward in time. The times that a spacecraft $sc_j \,|\, j = 1,..., N_{sc}$ of the constellation is in view of the surface asset located at (λ, L) represent opportunities to collect 2-Way Doppler measurements, and compute a surface asset position with associated covariance. For MPART, only the covariance $\mathbf{P}$ associated with the epoch state position of the surface asset $\vec{r}^{\,sa}(t_o)$ (the index i has been dropped for convenience) is needed. It is computed recursively using the following standard computations [3],

$$\mathbf{P}^+ = \mathbf{P}^- - \frac{\mathbf{P}^-\mathbf{h}\mathbf{h}^{\mathrm{T}}\mathbf{P}^-}{\sigma_{DR}^2 + \mathbf{h}\mathbf{P}^-\mathbf{h}^{\mathrm{T}}}, \tag{9}$$

where the measurements are processed as scalars ($\rightarrow \mathbf{h}\mathbf{P}^-\mathbf{h}^T$ is scalar valued), the superscript '+' refers to quantities after a measurement is processed, and '-' to quantities before measurement processing. The initial value for the recursion is $\mathbf{P}_o$ and is applied at epoch time $t_{o,j}$ The measurement geometry (column) vector $\mathbf{h}(t)$ associated with a measurement $DR(t)$ taken at time t between the surface asset and the in-view spacecraft sc_j is computed using,

$$\mathbf{h}(t) \equiv \frac{\partial DR(t)}{\partial \vec{r}^{\,sa}(t_{o,i})} = \left[\frac{\vec{r}^{\,sa}(t) - \vec{r}^{\,sc_j}(t)}{\rho(t)}\right]^T \mathbf{R}(t, t_{o,i}) - \left[\frac{\vec{r}^{\,sa}(t - T_c) - \vec{r}^{\,sc_j}(t - T_c)}{\rho(t - T_c)}\right]^T \mathbf{R}(t - T_c, t_{o,i}) \ , \tag{10}$$

and $\mathbf{R}(t, t_{o,i})$, defined as surface asset transition matrix, is determined as follows,

$$\mathbf{R}(t, t_{o,i}) = \begin{bmatrix} \cos\dot{\omega}_M(t - t_{o,i}) & -\sin\dot{\omega}_M(t - t_{o,i}) & 0 \\ \sin\dot{\omega}_M(t - t_{o,i}) & \cos\dot{\omega}_M(t - t_{o,i}) & 0 \\ 0 & 0 & 1 \end{bmatrix} , \tag{11}$$

where $\dot{\omega}_M$ is the mean rotation rate of Mars and the surface asset is assumed to be not moving. For this study the selected propagation (and sampling) period is set at a fixed 15 days. Empirical evidence from prior studies [1] suggests that this period leads to a nearly stationary value for the MPART statistic for low to mid-altitude orbits being considered. Future work will be directed towards determining quantitative measures that signify when sufficient data has been collected for the MPART statistic to become stationary. Note, that the propagation utilizes Kepler orbits being perturbed by secular oblateness terms. Hence, the orbit's semi-major axis, eccentricity, and inclination (a, e, i) remain constant, and the right ascension of the ascending node Ω and mean anomaly M angles vary linearly due to inverse square and oblateness effects.

Now the MPART statistic applies to a specific surface asset located at (λ, L) , in designing a spacecraft constellation it is necessary to assess the constellation's performance at providing positioning services to all latitudes and longitudes in its target coverage region. Furthermore, a fitness function (or metric) is needed that captures this global positioning performance, and can be used to compare *competing* constellation designs. To guide selection of this fitness function several design goals are defined,

1. The selected constellation orbits should provide positioning services to all potential surface assets in the targeted coverage region and do so with a minimal value for the MPART statistic for each surface asset covered;
2. The constellation orbits should minimize variations of the MPART statistic across all covered surface asset locations.

These design objectives lead to the following choice for a fitness function,

$$f = \langle MPART(\lambda, L) \rangle + STD\left[\langle MPART(\lambda, L) \rangle\right] , \tag{12}$$

where $\langle\rangle$ is the average operator that is taken over all surface asset locations, and $STD[\cdot]$ is the standard deviation associated with the computed average value. These are sample

statistics, thus the operators are implemented using finite sums associated with a discrete distribution of surface asset locations $\{(\lambda_p, L_q) \mid \text{surface asset } (p,q) \in N_{sa}\}$ where N_{sa} is the total number of surface assets. Since the present study is concerned with global coverage, that is restricted to circular orbit designs, it is sufficient to consider surface assets located only in one hemisphere. Furthermore to ensure a fair weighting at all longitudes and latitudes the surface assets should be distributed so that they are centered on equal spherical area patches. For this study, $N_{sa} = 109$ is selected which leads to an area patch of size .057 rad^2 ($= 2\pi / N_{sa}$) . It is now possible to define a design objective that is amenable to a numerical search, and captures the goals outlined previously, it is stated as follows:

Sparse Constellation Design Objective *For a constellation with a fixed small number of spacecraft N_{sc}, determine the spacecraft orbit parameters that minimize the value of the fitness function as defined in Eq. (12).*

The particulars of the constellation design space are specific to the scenario being explored (i.e., single satellite that is Sun Synchronous), and will be delineated for each scenario in the results section. Typically, the design space specifies ranges for parameters such as spacecraft altitude, inclination, and relative phasing of ascending nodes and mean anomalies between participating spacecraft.

OPTIMIZATION VIA GENETIC ALGORITHMS

The constellation design problem posed in the previous section has several complex characteristics including a fitness function that is not readily differentiable and statistical in nature; hence a gradient-based optimization method proves difficult to apply. As this is the case, non-gradient techniques such as, simulated annealing, genetic algorithm, downhill simplex, or a stochastic search are better suited. The genetic algorithm has been successfully applied to various constellation design problems [4, 5, 6], and recently to an adaptive navigation problem that utilizes a sample statistic for its fitness function [7]. Guided by these successes, a genetic algorithm (GA) is selected for the problem presented in this paper.

A GA is a computational representation of natural selection that bases its search and optimization on the analogy that an individual that is more fit to its environment is closer to an optimal design. Here the fitness of a specific constellation design is represented by the value obtained when evaluating Eq. [12]. The specific GA parameters and operators selected for use in the current study include,

1. A chromosome, representing an individual constellation design, that is represented as a binary string of N_{bits} in length and encoded using Gray coding. Each design scenario described in the Scenario Results section includes a description of the

selected design variables (plus the associated range of values), and the particular chromosome structure utilized.

2. A population size that is N_{POP} = (3xN_{bits} ± 1 to be even) and initialized with a random set of individuals. Recall that a population consists of N_{POP} individual constellation designs.
3. Uniform crossover,
4. Single-branch tournament selection,
5. Elitism (i.e., the best individual of the current generation is put into the next one),
6. Mutation with probability $P_m = \left|\frac{1}{N_{POP}} - \frac{1}{N_{bits}}\right| / 2 + \min\left(\frac{1}{N_{POP}}, \frac{1}{N_{bits}}\right)$,
7. A convergence criteria that if the best fitness value has not improved by more than 1/1000 after 15 generations, then the GA stops.

Detailed descriptions of these GA parameters and operators can be found in Refs. [4 and 7].

SCENARIO RESULTS

Sparse Constellations using Sun Synchronous, Circular Orbits

This scenario examines constellations consisting of 1 to 4 spacecraft that are constrained to be circular and Sun-synchronous. These conditions fix the inclination to have a particular value as determined by,

$$\cos i = -\frac{2}{3J_2}\left(\frac{n_{sun}}{n}\right)\left(\frac{a}{R_M}\right)^2, \quad n_{sun} = \frac{2\pi}{\text{Martian Year}} \quad \& \quad e \equiv 0, \tag{13}$$

where R_M is the mean radius of Mars, J_2 is the oblateness harmonic coefficient for Mars, and n is the spacecraft's mean motion. Use of Eq. (13) determines a physically realizable range of altitudes that has an upper limit of 5499 km, higher altitudes render Eq. (13) insoluble. Sun synchronous orbits are being investigated because they yield superior spacecraft and surface asset lighting conditions when link opportunities are present. Indeed, most recent Mars Network studies have focused attention on this orbital class. Future studies will expand the orbit space being searched by removing this constraint, and thus allowing inclination to vary freely. The lower bound for the altitudes range is set to 400 km. Again, this value is motivated because it is a standard orbit used by Mars orbiting science spacecraft (such as the Mars Global Surveyor or Mars Odyssey) [8]. In the multi-spacecraft cases, the altitudes are constrained to all have a common altitude. The other parameters in the search space include the node spacing between each

Table 1: GA results for the constellations of with 1 to 4 members, circular, and Sun-synchronous. Included for comparison are results for a Walker 5/5/1 constellation that has continuous, 1-fold, global coverage.

N_{sats}:	1	2	3	4	**Walker 5/5/1**
$\langle MPART \rangle$ (hrs)	2.354	1.119	0.717	0.560	1.006
STD (hrs)	0.130	0.036	0.030	0.025	0.028
f = MPART + STD (hrs)	2.483	1.155	0.747	0.585	1.034
Altitude (km)	3884.067	3682.918	3233.886	3124.123	6142.800
i (°)	119.721	116.708	110.935	109.696	43.660
$\Omega_2 - \Omega_1$ (°)	N/A	125.401	74.677	73.268	72.000
$\Omega_3 - \Omega_1$ (°)	N/A	N/A	310.685	293.777	144.000
$\Omega_4 - \Omega_1$ (°)	N/A	N/A	N/A	324.775	216.000
$\Omega_5 - \Omega_1$ (°)	N/A	N/A	N/A	N/A	288.000
$M_2 - M_1$ (°)	N/A	209.237	164.853	123.288	72.000
$M_3 - M_1$ (°)	N/A	N/A	196.556	229.667	144.000
$M_3 - M_1$ (°)	N/A	N/A	N/A	139.491	216.000
$M_5 - M_1$ (°)	N/A	N/A	N/A	N/A	288.000

spacecraft relative to the first in the constellation, and the mean anomaly spacing between each spacecraft and the first. Each instance of these variables can take values lying between 0 and 360°. Each variable in this simulation has a 9 bit binary string encoding for the GAs chromosome (except in the single satellite case where the altitude has a 10 bit representation). The resulting chromosomes have lengths that vary from 10 bits (1 spacecraft case) to 63 bits (= 9 bits x 7 variables for the 4 spacecraft case), and populations from 30 to 190 individual designs (using the 3 x N_{bits} and even valued rule).

The results for all the GA runs are tabulated in Table 1. Also included in the results are fitness values for a Walker 5/5/1 constellation. This Walker configuration is the smallest constellation at lowest altitudes consiting of circular orbits that provides continuous, single-fold coverage to the entire planet [9]. Consider the results for the single satellite case, global average MPART statistic $\langle MPART \rangle$ for this orbit is 2.354 hrs and the variation across all longitudes and latitudes is 0.13 hrs, recall that these values are associated with $RSS_{desired} = 1\,\text{m}$. It is informative to see the $\langle MPART \rangle$ values vary as function of latitude and longitude, this is shown in Figure 1. The figure illustrates that variations are small at most latitudes and longitudes and statistical in nature. There is a trend towards shorter MPART values at higher latitudes, however, the overall result is a small standard deviation across all latitudes and longitudes. Results of the complete GA

run for this scenario are shown in Figure 2. Also shown for comparison fitness values for the specific resonant orbits, which are included because they exhibit longitudinal biases that affect their fitness function values. The $\langle MPART \rangle$ values and their associated standard deviations (represented by the error bars) are plotted versus the altitude. The trend of the plot is for the $\langle MPART \rangle$ values and standard deviations to be smallest near the minimal value (i.e., the optimal single satellite result in Figure 1 and Table 1) with the largest values and deviations occurring at low and high altitudes. Note that there is a large range of altitudes (~ 1500 km to ~ 4500 km) where the fitness value remains below the 3 hr level and variations in the computed $\langle MPART \rangle$ values are small. Thus, even though the 3884 km case is best, these other orbits could be utilized as well with only minor penalties in navigation performance. Indeed, the current focus of the Mars Network has been directed towards an examination of orbits at the mid-4000 km altitudes. Other analysis has shown that these orbits yield significant advantages for communications performance. Clearly, the results presented here suggest that navigation performance to surface assets perform well in this altitude regime as well.

Results for constellations with 2, 3 and 4 spacecraft are tabulated as well. As expected, the $\langle MPART \rangle$ values reduce in value as the number of spacecraft increases. That is, as more spacecraft become available for collecting tracking data to the surface asset the average time it takes to achieve the 1 m threshold position accuracy decreases.

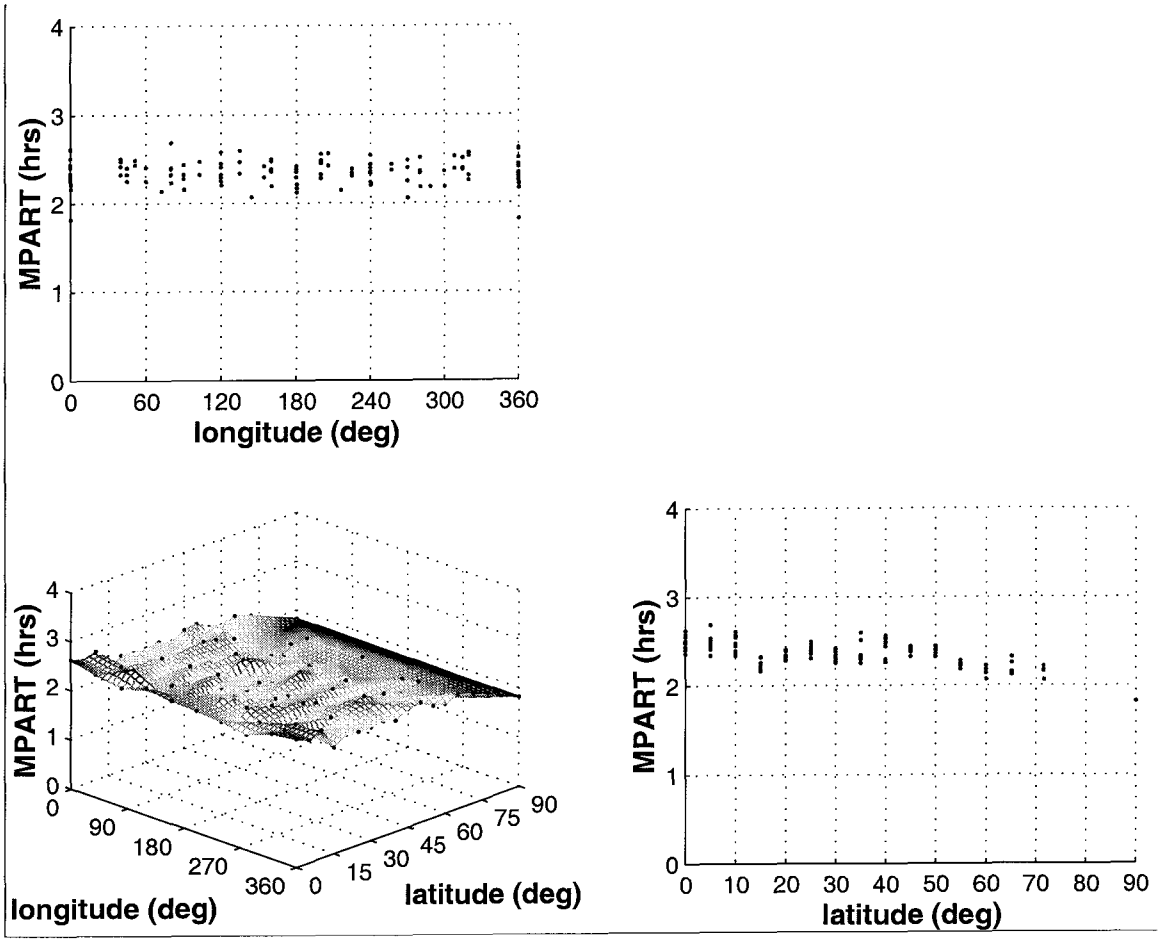

Figure 1: MPART results as a function of latitude and longitude with $RSS_{desired} = 1$ m for the best case single satellite circular Sun synchronous case (Altitude = 3884 km, Inclination = 119.7°). Each dot represents the value of MPART returned by the simulation tool for the surface asset located at that location (N_{sa} = 109). The global statistics for this case are $\langle MPART \rangle = 2.354$ hrs and the STD = 0.130 hrs.

Furthermore, note that the altitude of the constellations decreases as the number of spacecraft increases. These results are intuitive and consistent with constellation designs that are based on figures of merit relating to coverage properties only. The results for ascending node and mean anomaly do not yield a clear trend. This could be an artifact of the computation for the individual surface asset MPART statistics being sensitive to scenario parameters or initial conditions. This could also be representative of the fact that in the mid-altitude regime of orbits, the $\langle MPART \rangle$ statistic is nearly flat and variations in phasing cause little substantive change in the resulting values for the statistics. To address the first issue of sensitivity to scenario parameters and initial conditions, continued research is needed into computational techniques for ensuring that the returned values for the MPART statistic are stationary. Insight into the 'flatness' of the MPART

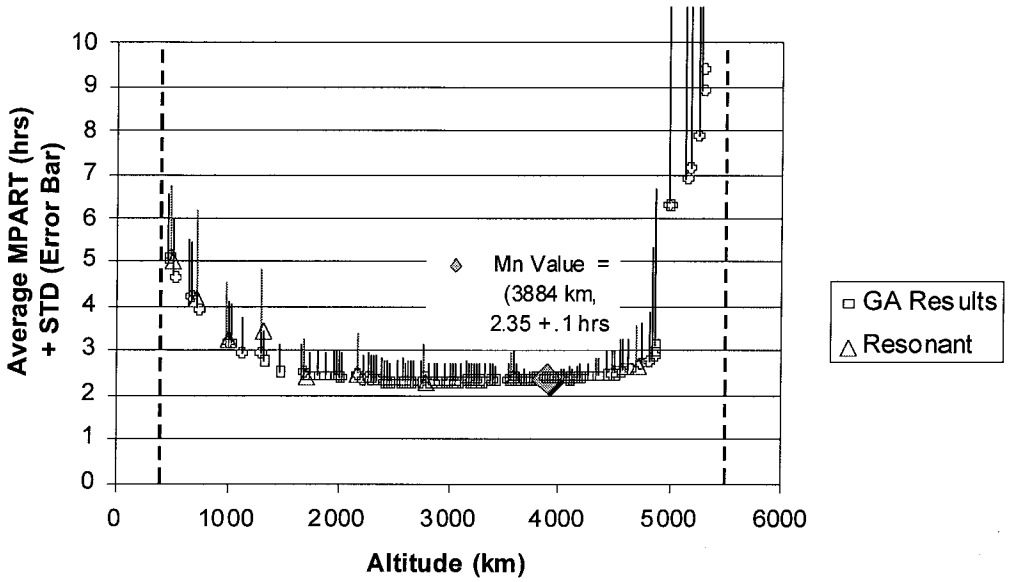

Figure 2: GA results from all generations for the case with a single satellite constrained to be Sun synchronous. The dashed vertical lines at 400 km and 5499 km represent the range of altitudes that were searched over. Note that results for the resonant altitude orbits are not part of the GA, and have been included for comparison with the typical non-resonant case that is returned by the GA.

statistic can be examined by refining the GAs search parameters so that the mid-altitude regime is explored more thoroughly via a tighter discretization. Again, these are likely areas for future work.

The most significant conclusion that can be ascertained for the multi-spacecraft results is from their comparison to the Walker 5/5/1 case. The Walker constellation MPART statistic takes a value of ~ 1 hr and lies between the MPART values associated with the GA's 2 spacecraft result (1.119 hrs) and the 3 spacecraft result (0.717 hrs). Also note that the GA results yield significantly lower altitudes, 2 spacecraft at 3683 km and 3 spacecraft at 3234 km altitude, than the Walker continuous coverage case at 6143 km. Clearly, continuous coverage yields no particular advantage for positioning performance using 2-Way Doppler data. Furthermore, the cost associated with fielding a Walker 5/5/1 constellation is significantly greater because it requires more spacecraft at higher altitudes ($\Rightarrow$ higher delta-V costs). Current studies into constellations that do not have the Sun-synchronous constraint have also found an example 2 satellite constellation at an even lower altitude (2525 km and inclination of 118°) with an associated MPART statistic of 1.1 hrs. The overall conclusion is that lower altitude sparse constellations providing discontinuous coverage can yield better surface asset positioning performance than a larger continuously in view constellation.

Table 2: GA search results for the two satellite constellation scenario with one satellite constrained to be in a Sun-synchronous, circular, 400 km orbit, and the other with parameters as shown.

$\langle MPART \rangle$ (hrs)	STD (hrs)	Fitness (hrs)	Altitude (km)	i (°)	$\Omega_2 - \Omega_1$ (°)	$M_2 - M_1$ (°)
1.583	.150	1.733	3692.896	116.851	271.937	19.726

Mars Network Example

This example considers a scenario that is being actively investigated for the Mars Network and consists of a two-satellite constellation. The first member of the network is a science spacecraft that has a telecommunications/navigation payload on board but that has orbital parameters constrained by the needs of the science instruments. The second spacecraft in the constellation, referred to as a *telesat*, has a primary mission of providing Mars Network telecommunications/navigation services. The orbital parameters for the second satellite can be optimized to provide these services. For the purposes of this study, a GA search is conducted to find an orbit that is best 'fit' at providing surface asset positioning services in combination with a science orbiter that is in a Sun-synchronous, circular, 400 km altitude orbit. This puts the science orbiter in a 92.9° orbit. The telesat is also fixed to be Sun-synchronous, but, as before, the altitude, relative ascending node, and relative mean anomaly are allowed to vary. For the GA, this selection yields a chromosome that is 27 bits in length (3 variables at 9 bits/variable), and a population that consists of 82 individuals. The ranges of values that can be taken by the variables are the same as before.

The results for this scenario are tabulated in Table 2. The resulting orbit has nearly the same altitude (and inclination) as that for the 2 satellite case in the prior scenario. The fitness value for the current scenario is larger by 35 min (~ 50%), indicating the current constrained constellation is not nearly as efficient as in the first case. However, the orbit is not substantially different (except for the nodal and mean anomaly phasing values). Note that since both of these orbits have a Sun-synchronous nodal rate their relative orientation remains fixed as the constellation orbit planes evolve in inertial space. The GA selected orbits have about a 270° separation, this spacing result warrants further investigation because it is suggestive of a symmetry that has not clearly revealed in these preliminary results.

CONSIDERING ORBIT ERROR

The preceding optimization studies use covariance computations, Eq. (9), that yield surface asset location uncertainties that have measurement noise as the only input error source. Doing so produces constellation designs that are selected for their superior

geometric qualities, however the values of the computed statistics are misleading in that they do not account for other significant error sources. Recent studies [1, 10] into Mars surface asset positioning have found that the most significant additional error source impacting location uncertainties is associated with the orbit error of the constellation spacecraft. Orbit errors can be represented conveniently in radial, transverse, and normal components (RTN) defined using a non-inertial coordinate system with origin at the current location of the spacecraft, and unit vectors defined as follows,

$$\begin{aligned} \hat{R} &= \frac{\vec{r}^{\,sc}}{r^{sc}} \\ \hat{N} &= \frac{\vec{r}^{\,sc} \times \dot{\vec{r}}^{\,sc}}{\left\| \vec{r}^{\,sc} \times \dot{\vec{r}}^{\,sc} \right\|}, \\ \hat{T} &= \hat{N} \times \hat{R} \end{aligned} \tag{14}$$

where for convenience the j has been dropped on the superscript spacecraft identifier sc_j, the '^' indicates a unit vector, and $\|\|$ is the magnitude operator. The error associated with a spacecraft location in its orbit is assumed to take the following simplified form,

$$E[\Delta\vec{r}^{\,sc}(\Delta\vec{r}^{\,sc})^T] = \begin{bmatrix} \sigma_R^2 & 0 & 0 \\ 0 & \sigma_T^2 & 0 \\ 0 & 0 & \sigma_N^2 \end{bmatrix}, \quad E[\Delta\dot{\vec{r}}^{\,sc}(\Delta\dot{\vec{r}}^{\,sc})^T] = \begin{bmatrix} \sigma_{\dot{R}}^2 & 0 & 0 \\ 0 & \sigma_{\dot{T}}^2 & 0 \\ 0 & 0 & \sigma_{\dot{N}}^2 \end{bmatrix}. \tag{15}$$

That is, the cross-correlated errors within and between RTN position and velocity components have been neglected. Using the definition of slant range it is possible to map orbit error, expressed as in Eq. (15), into a slant range rate error. First recall that the slant range rate can be expressed, using Eq. (1) as follows,

$$\dot{\rho} = \frac{\vec{\rho} \cdot \dot{\vec{\rho}}}{\rho} = \dot{\vec{\rho}} \cdot \hat{\rho} \tag{16}$$

Of interest is the variation of Eq. (16) with respect to the spacecraft state vector $(\vec{r}^{\,sc}, \dot{\vec{r}}^{\,sc})$. Taking this variation yields the following relationship,

$$\Delta\dot{\rho} \equiv \mathbf{h}_c^T \begin{pmatrix} \Delta\vec{r}^{\,sc} \\ \Delta\dot{\vec{r}}^{\,sc} \end{pmatrix} = \begin{bmatrix} \frac{\partial\dot{\rho}}{\partial\vec{r}^{\,sc}}, & \frac{\partial\dot{\rho}}{\partial\dot{\vec{r}}^{\,sc}} \end{bmatrix}^T \begin{pmatrix} \Delta\vec{r}^{\,sc} \\ \Delta\dot{\vec{r}}^{\,sc} \end{pmatrix} = \frac{1}{\rho}\left(\dot{\vec{\rho}} - \dot{\rho}\hat{\rho}\right) \Delta\vec{r}^{\,sc} + \hat{\rho} \cdot \Delta\dot{\vec{r}}^{\,sc}. \tag{17}$$

where $\Delta\vec{r}^{\,sc} = \Delta R\hat{R} + \Delta T\hat{T} + \Delta N\hat{N}$ and $\Delta\dot{\vec{r}}^{\,sc} = \Delta\dot{R}\hat{R} + \Delta\dot{T}\hat{T} + \Delta\dot{N}\hat{N}$, and $\mathbf{h}_c$ identifies the column vector of partials relating slant range rate to the spacecraft state. Now, assuming RTN orbit errors are as specified in Eq. (15), the slant range rate error due to orbit error can be formulated and takes the form,

$$\sigma_{\dot{\rho}}^2 = E[\Delta\dot{\rho}\Delta\dot{\rho}] = \left[\frac{\partial\dot{\rho}}{\partial\vec{r}^{sc}}, \frac{\partial\dot{\rho}}{\partial\dot{\vec{r}}^{sc}}\right]^T \begin{pmatrix} \Delta\vec{r}^{sc} \\ \Delta\dot{\vec{r}}^{sc} \end{pmatrix}$$

$$= \frac{1}{\rho^2}(\dot{\vec{\rho}}\cdot\hat{R} - \dot{\rho}\hat{\rho}\cdot\hat{R})^2\sigma_R^2 + \frac{1}{\rho^2}(\dot{\vec{\rho}}\cdot\hat{T} - \dot{\rho}\hat{\rho}\cdot\hat{T})^2\sigma_T^2 + \frac{1}{\rho^2}(\dot{\vec{\rho}}\cdot\hat{N} - \dot{\rho}\hat{\rho}\cdot\hat{N})^2\sigma_N^2 + \tag{18}$$

$$(\vec{\rho}\cdot\hat{R})\sigma_{\dot{R}}^2 + (\vec{\rho}\cdot\hat{T})\sigma_{\dot{T}}^2 + (\vec{\rho}\cdot\hat{N})\sigma_{\dot{N}}^2 \quad .$$

So far these computations have made no assumption regarding the time dependency of the RTN orbit errors $[\sigma_R, \sigma_T, \sigma_N, \sigma_{\dot{R}}, \sigma_{\dot{T}}, \sigma_{\dot{N}}]$. In a simplified orbit error treatment the RTN errors can be conservatively fixed as constants and given values that are upper bounds of the observed errors determined from high fidelity orbit error analyses. This is the approach taken in the current research. A more sophisticated approach that maps gravity field errors (the largest orbit error contributor for many Mars orbiters[10]) into the orbit error is currently under investigation.

To arrive at appropriate values for $[\sigma_R, \sigma_T, \sigma_N, \sigma_{\dot{R}}, \sigma_{\dot{T}}, \sigma_{\dot{N}}]$ consider the example of a 400 km altitude, circular, Sun-synchronous orbit that is being tracked with DSN (Deep Space Network) 2-Way Doppler and range data. The analysis assumes the error sources and error levels as indicated in Table 3 plus the filtering assumptions. The simulation is run for 5 days with the resulting RTN errors and RTN rate errors as shown in Figure 3. The results clearly illustrate that the errors are bounded and exhibit a minor growth (that is attributable to a stale nominal orbit – reinitializing the nominal would arrest this growth). The results of this simulation yield errors that can be bound as follows,

$$[\sigma_R, \sigma_T, \sigma_N, \sigma_{\dot{R}}, \sigma_{\dot{T}}, \sigma_{\dot{N}}] = [1\text{ m}, 6\text{ m}, 3\text{ m}, 4\text{ mm/s}, 1\text{ mm/s}, 3\text{ mm/s}] \ ,$$

with an overall RSS position error of ~ 7.3 m, and RSS velocity error of ~ 5 mm/s. Selected additional simulations throughout a Martian year exhibit RSS levels that are less than 11 m in position and 8 mm/s in velocity. As another sample, analysis using a 4450 km circular, Sun-synchronous orbit also yield levels that are similar with overall RSS position error of ~ 10 m, and RSS velocity errors ~ 4 mm/s. All of the examined cases can be conservatively bounded by an RSS of 20 m in position and 10 mm/s in velocity. These levels are selected for the subsequent analysis and distributed equally between components to produce the following distribution,

$$[\sigma_R, \sigma_T, \sigma_N, \sigma_{\dot{R}}, \sigma_{\dot{T}}, \sigma_{\dot{N}}] = [11\text{ m}, 11\text{ m}, 11\text{ m}, 5.7\text{ mm/s}, 5.7\text{ mm/s}, 5.7\text{ mm/s}] \ . \tag{19}$$

These values are fixed and can be incorporated into Eq. (18), which yields a time dependent value for the slant range rate error $\sigma_{\dot{\rho}}(t)$. This error is evaluated on receipt of a measurement at time *t*. A conservative technique for providing an upper bound on the

Table 3: Covariance analysis assumptions to determine representative levels of RTN orbit errors. Note that all input uncertainties identified in the table are 1σ levels

- Tracking with 2-Way range and Doppler between Goldstone and orbiter
  - Doppler noise at .1 mm/s @ 60 sec, range noise at 3 m every 30 min
  - Tracking for 5 days when in-view and at a 15° elevation angle cutoff. This yields about a 10 hr pass/day.
- Spacecraft/Orbit characteristics
  - 400 km circular orbit, circular, Sun-synchronous inclination
  - 700 kg satellite with 12.6 m^2 frontal area
- Filtering Assumptions
  - Position component aprioris at 10 km & velocity aprioris at 1 m/s
  - GM errors considered with apriori of .008581 km^3/sec^2
  - Gravity errors considered
    - Dynamics propagated with 75x&75 MGS 75c field
    - Included errors tuned for orbit (140 terms) - consist typically of all zonals and most uncertain near resonant tesserals
  - Solar radiation pressure considered with a 10% uncertainty
  - Momentum desaturations events estimated
    - Occur every 48 hrs with a spherical error of .173 mm/s
  - The following errors are considered as well at the indicated levels:
    - UTC-UT1 error ~ 15 cm,
    - XY Pole Wander ~ 10 cm,
    - Troposphere ~ 5 cm (Wet/Dry)
    - Ionosphere $5x10^{16}$ elec/m^2

contribution of orbit error in determining a surface assets position is to *consider* the error. Considering orbit error produces a covariance $\mathbf{P}_c$ that can be written as,

$$\mathbf{P}_c = \mathbf{P}^+ + \mathbf{S}\Sigma\mathbf{S}^T , \tag{20}$$

where $\mathbf{P}^+$ is the result of the computation in Eq. (9), $\Sigma = diag\left[\sigma_R^2, \sigma_T^2, \sigma_N^2, \sigma_R^2, \sigma_T^2, \sigma_N^2\right] \times T_c^2$ (note that the count time is included so that the range rate can derivatives are compatible with the range difference implementation), and the sensitivity matrix is expressed as,

$$\mathbf{S} = -\frac{\mathbf{P}^+\mathbf{h}^T\mathbf{h}_c}{\sigma_{DR}^2} . \tag{21}$$

Note that for Eq. (21) to be valid the measurements need to be processed as scalars. Using this fact and making a few manipulations, the covariance matrix that considers orbit error at the time of the measurement can be written in the following convenient form,

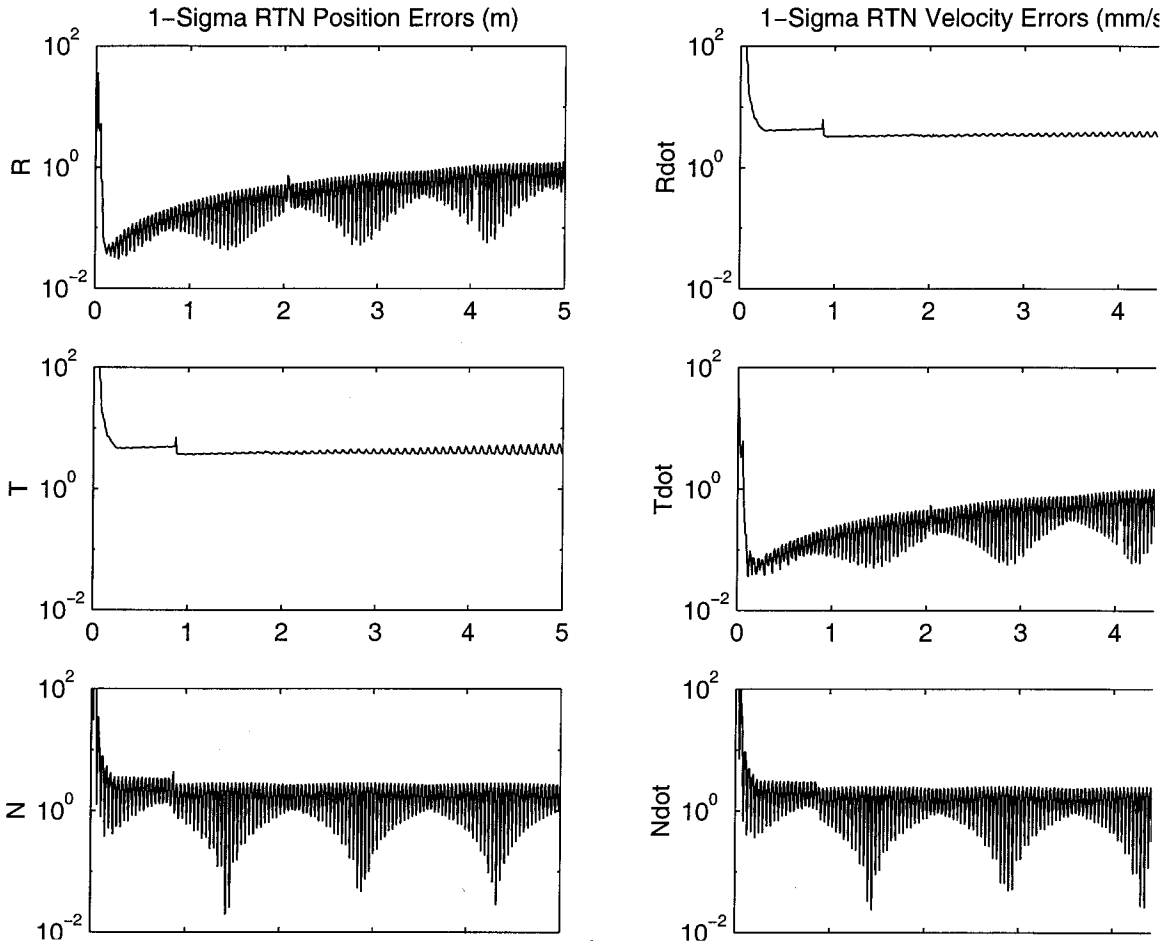

Figure 3: Orbit error results for a 5 day simulation of a Mars orbiter in a 400 km, Sun-synchronous, circular orbit.

$$\mathbf{P}_c^+ = \mathbf{P}^+ + \left(\frac{\mathbf{P}^+\mathbf{h}}{\sigma_{DR}}\right)\left(\frac{\mathbf{P}^+\mathbf{h}}{\sigma_{DR}}\right)^T\left(\frac{\sigma_\rho^{orbit}T_c}{\sigma_{DR}}\right)^2 \tag{22}$$

The equation expressed in this fashion exhibits superior numerical stability over other ways of implementing it. That is, performing the mathematical operations in the order prescribed by the parentheses yields a consider covariance matrix $\mathbf{P}_c^+$ that retains symmetry to high precision. Now for the recursion to proceed, the output matrix in Eq. (22) serves as the input matrix to Eq. (9) when another measurement is received.

Using preceding sequence of operations, the effect of orbit error on surface asset positioning can be examined as it relates to the MPART statistics. The value of $RSS_{desired}$ has been increased to 20 m (from 1 m) to be consistent with the orbit error at the levels defined in Eq. (19). Two examples are simulated. The first case is the single

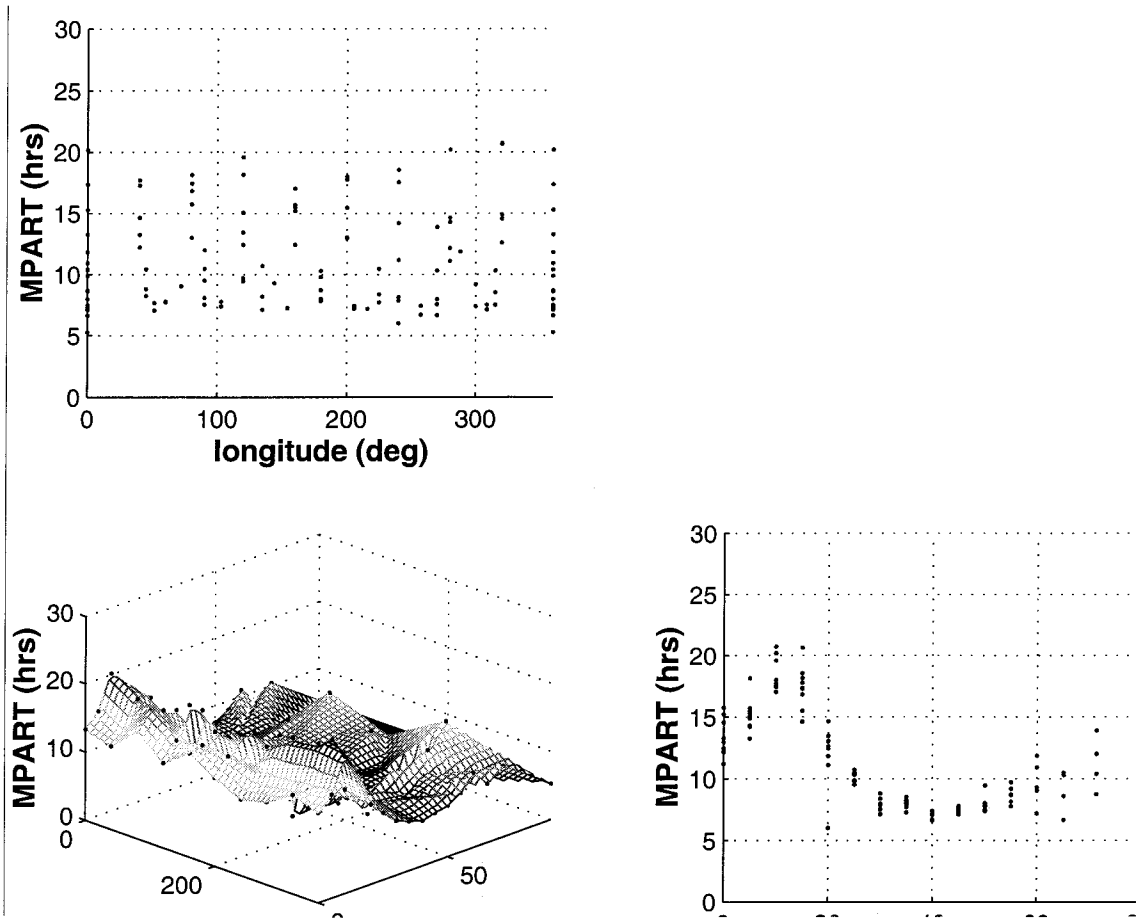

Figure 4: MPART results as a function of latitude and longitude with $RSS_{desired} = 20$ m for the best case single satellite circular Sun synchronous case (Altitude = 3884 km, Inclination = 119.7°) and *the orbit error is considered.* Each dot represents the value of MPART returned by the simulation tool for the surface asset located at that location (N_{sa} = 109). The global statistics for this case are $\langle MPART \rangle$ = 11.320 hrs and the STD = 4.056 hrs.

satellite

result from the first scenario (i.e., circular and sun-synchronous), with the results shown in Figure 4. The associated global statistics are $\langle MPART \rangle$ = 11.320 hrs and the STD = 4.056 hrs. These values represent a marked increase over the case with only data noise and, comparing to Figure 1, the variations across latitudes are greater (hence the larger relative value for STD). The second case is from the Mars Network scenario where one satellite is fixed at 400 km and the other orbit is optimized to return a minimal fitness value. The results are exhibited in Figure 5, and have global statistics of $\langle MPART \rangle$ = 9.201 hrs and STD of 2.508 hrs. These results represent an improvement over the single

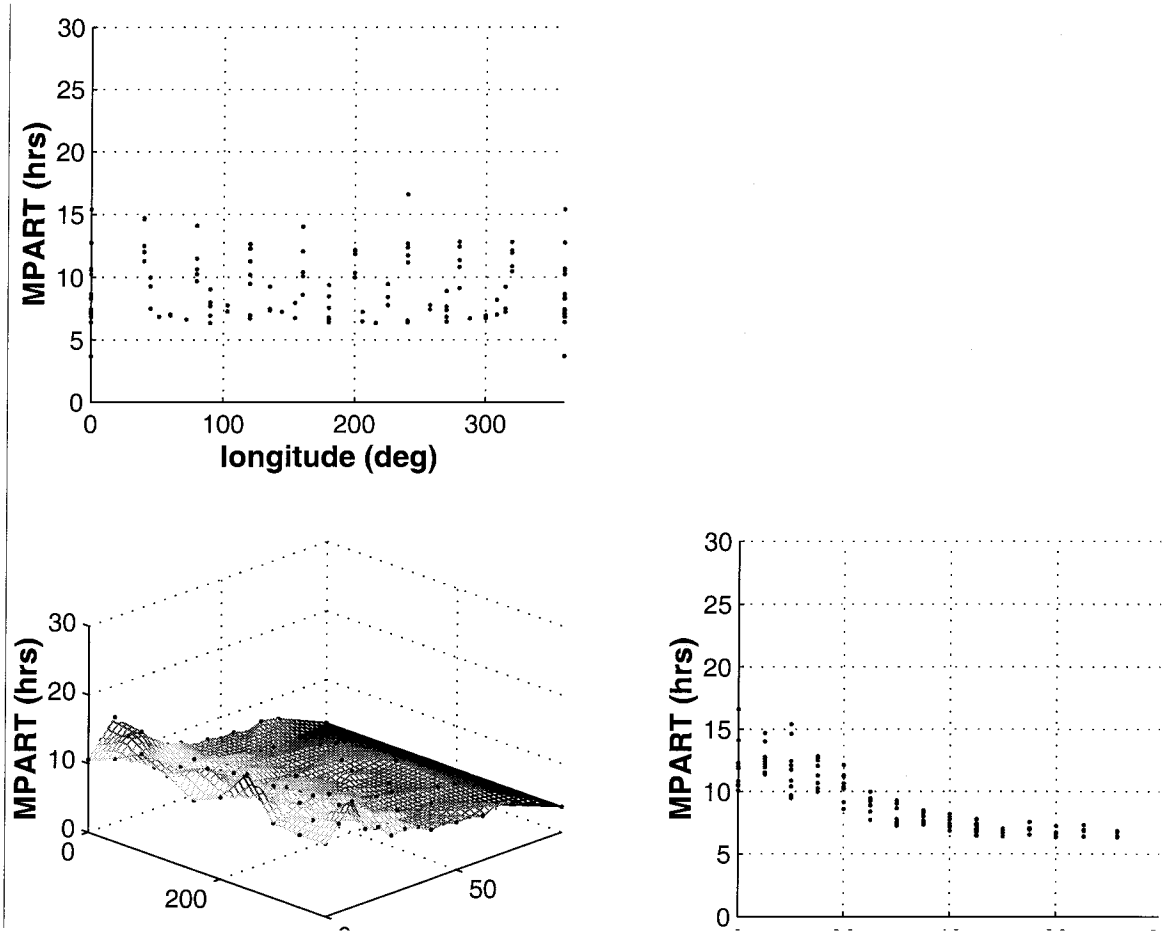

Figure 5: MPART results as a function of latitude and longitude with $RSS_{desired} = 20$ m for the Mars Network case with one satellite at a 400 km, Sun-Synchronous, circular orbit and the other found by the GA that is circular with altitude = 3692 km and sun-sync inclination = 116.9°. *The orbit error is considered.* Each dot represents the value of MPART returned by the simulation tool for the surface asset located at that location (N_{sa} = 109). The global statistics for this case are $\langle MPART \rangle$ = 9.201 hrs and the STD is 2.508 hrs.

telesat case, Figure 4, because the $\langle MPART \rangle$ value is not only smaller but latitudinal variations are less. Both cases exhibit a worst-case performance near the equator. This was not seen previously in Figure 1. It can be concluded that near the equator both of these constellations exhibit positioning services that are sensitive to orbit error.

CONCLUSIONS

An efficient technique for evaluating global performance of a constellation at providing surface asset positioning services was developed. The method centered around the MPART statistic which is a measure of average time it takes for a constellation to

determine the position accuracy of surface assets to some prescribed level. This metric was then utilized to determine sparse constellations at Mars (i.e., those with discontinuous coverage) that minimize a fitness value associated with the global average MPART statistic. The results show that, for circular and Sun-synchronized orbits, medium altitudes (~ 3000 to ~ 4000 km) are most efficient for constellations ranging in size from 1 to 4 satellites. Phasing results for the multi-satellite cases remain ambiguous; this is an area for further research. An important conclusion from these studies is that the global coverage constellation (Walker 5/5/1) has no particular advantage over the discontinous coverage cases. Indeed, since it is a larger constellation at higher altitudes, it is disadvantageous from a cost perspective. Finally, orbit error effects were considered in computing the MPART statistics. Not unexpectedly, MPART values increased, but most notably positioning services were most sensitive to these errors near the equator for the constellations found in this study.

Continuing efforts are focused on developing methods to ensure that MPART statistics are stationary, and developing more sophisticated techniques for incorporating orbit error. With these improvements, optimization studies oriented towards orbital phasing issues for sparse constellations can receive further attention.

ACKNOWLEDGEMENTS

This work was carried out at the Jet Propulsion Laboratory, California Institute of Technology, under contract with the National Aeronautics and Space Administration. The author would like to thank Joseph Guinn, David Bell, and Charles Edwards for the helpful input and discussions on this paper and with Mars Network constellation design, in general.

REFERENCES

1. ELY, T. A., ANDERSON, R. L., BAR-SEVER, Y. E, BELL, D. J., GUINN, J. R., JAH, M. K., KALLEMEYN, P. H., LEVENE, E. D., ROMANS, L. J., AND WU, S-C. "Mars Network Constellation Design Drivers and Strategies," AAS/AIAA Astrodynamics Specialist Conference Paper AAS 99-301, Girdwood, Alaska, August 16–18, 1999.
2. MOYER, T. D. "Mathematical Formulation of the Double-Precision Orbit Determination Program (DPODP)," JPL Technical Report 32-1527, May 15, 1971.
3. BATTIN, R. H. *An Introduction to the Mathematics and Methods of Astrodynamics*, AIAA Education Series, American Institute of Aeronautics and Astronautics, 1987.
4. ELY, T. A., CROSSLEY, W. A., WILLIAMS, E. A. "Satellite Constellation Design for Zonal Coverage Using Genetic Algorithms," The Journal of the Astronautical Sciences, Vol 47, Nos. 3 and 4, July – December 1999, pp. 207 – 228.

5. GEORGE, E., "Optimization of Satellite Constellations for Discontinuous Global Coverage via Genetic Algorithms," AAS Paper 97-621, AAS/AIAA Astrodynamics Specialist Conference, Sun Valley, ID, Aug. 4-7, 1997.

6. FRAYSSINHES, E., "Investigating New Satellite Constellation Geometries with Genetic Algorithms," AIAA Paper 96-3636, *Proceedings of the AIAA/AAS Astrodynamics Specialist Conference*, San Diego, CA, Jul. 1996, pp. 582-588.

7. ELY, T. A., BISHOP, R. H., CRAIN, T. P., "Adaptive Interplanetary Navigation Using Genetic Algorithms," to appear in *The Journal of the Astronautical Sciences*, Vol. 48, Nos. 2 and 3, April – September 2000.

8. JPL Current Missions Webpage, http://www.jpl.nasa.gov/missions/.

9. BALLARD, A. H. "Rosette Constellations of Earth Satellites," *IEEE Transactions on Aerospace and Electronic Systems*, Vol. AES-16, No. 5, Sept. 1980, pp. 656 – 673.

10. GUINN, J. R., ELY, T. A., PORTOCK, B. "Mars Surface Asset Positioning Using In-Situ Radio Tracking," AAS/AIAA Space Flight Mechanics Meeting AAS 01-100, Santa Barbara, California, February 11 – 14, 2001.